

Space Vector Control of a Permanent Magnet Linear Synchronous Motor Based on the Improved Single Neuron PID Algorithm

Shuangbao Shu, Yuzhong Zhang, Xiaoxu Wang, Qiaosheng Pan, Xiaojie Tao

School of Instrument Science and Opto-electronics Engineering, Hefei University of Technology, Hefei, 230009, China. (e-mail: zhangyuzhong@hfut.edu.cn).

Abstract: There are some characteristics of a Permanent Magnet Linear Synchronous Motor (PMLSM) such as nonlinearity, strong coupling, and multi-control variables, etc. The traditional Proportional Integral Derivative (PID) control is not suitable for dealing with the nonlinear and time-varying system due to its fixed control parameters. Therefore, the PMLSM control algorithm is designed in this paper based on Space Vector Pulse Width Modulation (SVPWM), by optimizing the traditional principle model of a PMLSM and using the improved single neuron PID. According to the structure and the working principle of the PMLSM, the mathematical model is set up by using the space vector control method and the coordinate transformation, and the corresponding control system is built by SVPWM with $i_d = 0$ methods. Combining biological immune regulation with a single neuron PID control algorithm, and learning from immune regulation with the capability of eliminating antigen and stabilizing immune system, the improved single neuron PID is proposed. With the advantages of improving the learning speed of the neuron algorithm, on-line adjustment of the proportional coefficient value and optimizing control algorithm, the control algorithm of the PMLSM is constructed. Experiment results show that the improved single neuron PID method has the advantages of faster response, higher control precision, good adaptability and robustness compared with the ordinary single neuron PID control.

Keywords: PMLSM, motor control, space vector control, pulse width modulation, single neuron PID, immune regulation.

1. INTRODUCTION

A linear motor is a kind of electric power transmission device that converts electric energy into linear motion mechanical energy directly. Compared with the traditional rotary motor, a linear motor eliminates many intermediate transmission mechanisms and has some advantages such as high sensitivity, large thrust force and large acceleration, and thus is widely used. The research mainly focusing on drive and servo control technology of linear motor also attracts a large number of engineering experts and research institutes (Boldea and Nasar, 1999; Hellinger and Mnich, 2009; Yan, 2009; An, et al., 2013; Tang and Duan, 2018). Because a Permanent Magnet Linear Synchronous Motor (PMLSM) is a typical multivariate and nonlinear system with strongly coupling (Kim, et al., 2012; Dang et al., 2013; Ilten and Demirtas, 2016; Cash and Olatunbosun, 2017; Giernacki et al., 2018; Torres et al., 2019; Bahmanpour et al., 2019), the stability and accuracy of the control system may be reduced due to various factors during the control process. Some factors, such as end effects, cogging effects, thrust fluctuations, etc., bring difficulties to precise control. Therefore, the traditional Proportional Integral Derivative (PID) control cannot perfectly meet the demands of the control system (Jones et al., 1996; Durand et al., 2018). At present, many intelligent control methods have been proposed, such as single neuron PID control, fuzzy PID control and PID control based on genetic algorithm, sliding mode control, etc (Marzi, 2005; Setayeshi et al., 2017; Pelc,

2014; Jia et al., 2015; Giernacki and Sadalla, 2017; Saleem et al., 2017; Bashir et al., 2019; Saleem et al., 2019; Ullah et al., 2019). However, among the above methods, parameters of the fuzzy PID control algorithm must be decided by prior experience that will be interference by strong subjectivity. Single neuron PID control has the problem of slow learning speed and long response time. Moreover, PID control based on a genetic algorithm requires the establishment of a precise model of the controlled object, which is hard to achieve in practical engineering applications.

The PMLSM control system in practical applications not only needs to meet the characteristics of high speed, high precision, and fast response but also needs to consider the stability and robustness of linear motor operation. This paper firstly analyses the perturbations of thrust and friction existing in a PMLSM. Based on the principle of vector coordinate transformation, the mathematical model is established and a control system based on Space Vector Pulse Width Modulation (SVPWM) is constructed. And then the improved single neuron PID control algorithm is designed, which combines biological immune regulation mechanism with single neuron PID control. The value of neuron proportional coefficient will be adjusted online based on the immune regulation with the capability of eliminating antigen rapidly and stabilizing the immune system, which makes the system possess the ability of fast response. The experimental results show that the control system with this method has a better control effect and dynamic performance.

The rest of the present paper is organized as follows. In section 2, the optimized mathematical PMLSM model is introduced, and the PMLSM control based on space vector pulse width modulation (SVPWM) with $i_d = 0$ methods is presented. An improved single neuron PID control algorithm is designed in detail in section 3. Section 4 provides the experimental results and discussions. The conclusion is given in the last section.

2. THE OPTIMIZED PMLSM CONTROL MODEL

2.1 Mathematic model of a PMLSM

A PMLSM has the thrust fluctuation due to its structural and principle characteristics. The main causes of the thrust fluctuation includes cogging effect and ends effect caused by the iron core slotting, viscous friction caused by the movement of the mover and sliding frictional disturbances and ripple disturbances due to non-uniform magnetic fields of the permanent magnets and unequal distribution of coil windings (Butt et al., 2004; Biswas et al., 2013; Butt and Rahman, 2013).

The main variables of the mathematical model of the motor in the three-phase stator coordinate system include three-phase voltages $u_a, u_b,$ and u_c , three-phase currents $i_a, i_b,$ and i_c , and stator winding flux chains $\psi_a, \psi_b,$ and ψ_c (Wei et al., 2009). The voltage equations and the flux linkages are expressed as follows:

$$\begin{cases} u_a = p\psi_a + Ri_a \\ u_b = p\psi_b + Ri_b \\ u_c = p\psi_c + Ri_c \end{cases} \quad (1)$$

$$\begin{bmatrix} \psi_a \\ \psi_b \\ \psi_c \end{bmatrix} = \begin{bmatrix} L & 0 & 0 \\ 0 & L & 0 \\ 0 & 0 & L \end{bmatrix} \begin{bmatrix} i_a \\ i_b \\ i_c \end{bmatrix} + \psi_f \begin{bmatrix} \cos\theta \\ \cos(\theta - \frac{2\pi}{3}) \\ \cos(\theta + \frac{2\pi}{3}) \end{bmatrix} \quad (2)$$

where p is the differential operator; R is the resistance of each phase winding; L is the three-phase winding inductance and ψ_f is the equivalent flux linkage of the permanent magnet. According to the analysis, the magnetic flux in the mathematical model of the PMLSM in the three-phase stator coordinate system has uncertainty and the thrust equation is based on the current equation and the flux linkage matrix, so it is difficult to use in the practical application of mathematical modelling.

Based on the mathematical model under the three-phase stator coordinate system, the mathematical model of the corresponding two-phase stator coordinate system can be obtained by using the coordinate transformation principle. The main variables include the voltages of u_α and u_β in the α - β coordinate system, the currents i_α and i_β , the stator winding flux linkages ψ_α and ψ_β , the resistance of each phase winding R , the inductance of each phase winding L , the pole pitch τ , the pole pair p_n , and the motor speed v_m . The voltage equations are expressed as follows:

$$\begin{cases} u_\alpha = Ri_\alpha + p\psi_\alpha \\ u_\beta = Ri_\beta + p\psi_\beta \end{cases} \quad (3)$$

For better understanding, the voltage equation can be further expressed as:

$$\begin{cases} u_\alpha = Ri_\alpha + pLi_\alpha - \frac{\pi}{\tau} p_n \psi_f v_m \cos\theta \\ u_\beta = Ri_\beta + pLi_\beta + \frac{\pi}{\tau} p_n \psi_f v_m \sin\theta \end{cases} \quad (4)$$

The flux linkage equation is:

$$\begin{cases} \psi_\alpha = Li_\alpha + \psi_f \cos\varphi \\ \psi_\beta = Li_\beta + \psi_f \sin\varphi \end{cases} \quad (5)$$

The corresponding electromagnetic thrust equation is:

$$F = \frac{3}{2} p_n \frac{\pi}{\tau} (\psi_\alpha i_\beta - \psi_\beta i_\alpha) \quad (6)$$

To establish the PMLSM model, the mathematical model under the two-phase moving sub-coordinate system is applied, and the mathematical equations and d - q coordinate transformation are used to analyze the mathematical model. The d - q coordinate system will be described later. The voltage equations in the d - q coordinate system can be described as follows:

$$\begin{cases} u_d = Ri_d + p\psi_d - \omega\psi_q \\ u_q = Ri_q + p\psi_q - \omega\psi_d \end{cases} \quad (7)$$

$$\begin{cases} \psi_d = L_d i_d + \psi_f \\ \psi_q = L_q \\ \psi_0 = L_{s0} i_0 \end{cases} \quad (8)$$

According to the above equation, the state equation can be obtained:

$$\begin{cases} \frac{di_d}{dt} = -\frac{R_s}{L_d} i_d + \frac{L_q}{L_d} \omega i_q + \frac{u_d}{L_d} \\ \frac{di_q}{dt} = -\frac{L_d}{L_q} \omega i_d - \frac{R_s}{L_q} i_q + \frac{u_q}{L_q} - \frac{\psi_f}{L_q} \omega \end{cases} \quad (9)$$

Total input power equation is:

$$P_{dq0} = \frac{3}{2} u_d i_d + \frac{3}{2} u_q i_q + 3u_0 i_0 \quad (10)$$

Substituting (4) and (5) into (10), we can obtain:

$$\begin{aligned} P_{dq0} = & \frac{3}{2} R_s (i_d^2 + i_q^2 + i_0^2) + \frac{3}{2} (i_d p\psi_d + i_q p\psi_q + i_0 p\psi_0) \\ & + \frac{3}{2} \omega (\psi_d i_d - \psi_q i_q) \end{aligned} \quad (11)$$

The three items in the (11) represent the armature equivalent winding resistance loss, the change in the magnetic field caused by the armature current, and the electromagnetic power involved in the energy conversion of the motor.

Electromagnetic power can be expressed as:

$$P_{em} = \frac{3}{2} \omega [\psi_f i_q + (L_d - L_q) i_d i_q] \quad (12)$$

The equation includes the electromagnetic power caused by the interaction between the secondary exciting magnetic field and the primary armature current and the reluctance electromagnetic power caused by the combination of the primary and secondary reluctance and the current component.

The electromagnetic thrust equation is:

$$\begin{aligned} F_{em} &= \frac{P_{em}}{v} = \frac{3\omega}{2v} [\psi_f i_q + (L_d - L_q) i_d i_q] \\ &= \frac{3\omega}{2\tau} [M_0 I_f i_q + (L_d - L_q) i_d i_q] \end{aligned} \quad (13)$$

where $\omega = \pi v / \tau$ and $\psi_0 = M_0 I_f$. For PMLSMs with different structures, such as salient-pole and hidden-pole, the thrust expressions are:

$$F_{em} = \frac{P_{em}}{v} = p_n \frac{3\omega}{2v} [M_0 I_f i_q + (L_d - L_q) i_d i_q] \quad (14)$$

$$F_{em} = p_n \frac{3\omega}{2\tau} \psi_f i_q = p_n \frac{3\omega}{2\tau L_s} |\psi_s| \psi_f \sin \delta \quad (15)$$

According to the above analysis, the mathematical model of the PMLSM in the two-phase moving element coordinate system can be obtained:

$$\begin{cases} u_d = R i_d + p i_d L_d - \omega L_q i_q \\ u_q = \omega L_d i_d + p i_q L_q + R i_q + \omega \psi_f \\ F_{em} = \frac{3}{2} p_n \pi \psi_f i_q / \tau \end{cases} \quad (16)$$

The motor's equation of motion is:

$$F_c = F_L + B_v v + M p v \quad (17)$$

where F_c is the electromagnetic thrust. F_L is the load resistance. B_v is the viscous friction coefficient and M is the quality of mover.

2.2 Space vector control design

Space vector control is an effective control method for the PMLSM control system (Oto et al., 2019; Ramasamy et al., 2018; Wang and Howe, 2004). The $i_d = 0$ control method has good applicability and can effectively guarantee control precision and rapidity. The core idea of this vector control is to set the d -axis current to zero in the stator winding so that the remaining q -axis current components are easy to control. Thus, the electromagnetic thrust equation of the mathematical model of the linear motor can be simplified as follows:

$$F_{em} = p_n \frac{3\omega}{2\tau} \psi_f i_q \quad (18)$$

It can be seen that the $i_d = 0$ vector control makes the electromagnetic thrust of the motor can be calculated from the shaft current and other variables such as motor torque obtained accordingly. This method can not only weaken the additional influence of the excitation current on the permanent magnet, improve the stability of the system, but also obtain a sufficient electromagnetic torque with the limited current. In addition, the stator required current is small with this control method, and the system loss can be effectively reduced.

However, vector control only solves the target output of the control system, that is, controls the three-phase voltage, and cannot complete the operation control of the motor. In practical applications, linear motors use inverters to achieve Direct Current (DC) to Alternating Current (AC) conversion, and the control algorithm outputs a critical transition to the inverter control pulse, which requires voltage modulation technology to be completed. Pulse Width Modulation (PWM) is widely used in this field (Shankar and Devi, 2019). The schematic diagram of the three-phase voltage inverter used in this system is shown in Fig.1, including six switch tubes, which correspond to the six PWM waveform control signals. The upper arm and the lower arm switch tubes in each phase of the three-phase full-bridge always have a complementary relationship with their control signals; that is, one switch is turned on, the signal is "1", and the other switch is turned off, the signal is "0". By combining the three-phase full-bridge switching states, there are eight voltage switching states, namely 000, 001, 010, 011, 100, 101, 110, and 111. In the 000 and 111 states, the inverter output is zero. Therefore these two states are called zero vector states. If the six basic vector states are evenly distributed in a certain order, a voltage space vector trajectory shaped like a regular hexagon can be obtained, as shown in Fig.2. Further, the regular hexagonal space vector can be used as a basis, and the space vector trajectory is gradually improved and approximated to a circular trajectory according to vector synthesis, thereby realizing the expected target of SVPWM modulation.

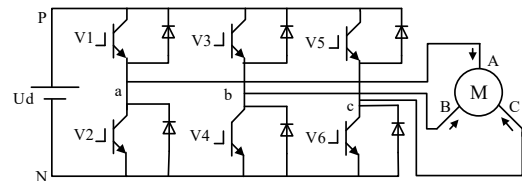


Fig. 1. Schematic diagram of the three-phase inverter.

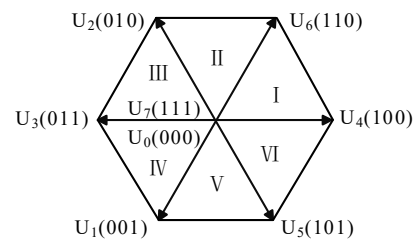


Fig. 2. Voltage space vector trajectory.

To achieve space vector PWM, the inverter output needs to be consistent with a certain composite reference voltage vector at any time. The voltage vector decomposition is shown in Fig.3. The resultant voltage vector can be obtained by respectively applying two adjacent basic voltage vectors U_x and U_{x+60° for a certain time. In order to reduce the number of switching of the inverter device, two adjacent basic voltage space vectors are selected for synthesis. In Fig.3, U_x and U_{x+60° are the adjacent two vectors. T_1 and T_2 are the action times of U_x and U_{x+60° , respectively, and U_{out} is the composite voltage space vector. In addition, in consideration of reducing the number of switching time as much as possible, only two adjacent voltage vector spaces are selected in vector synthesis. Specifically, steps such as sector determination, voltage vector action time calculation, and vector switching point calculation are required.

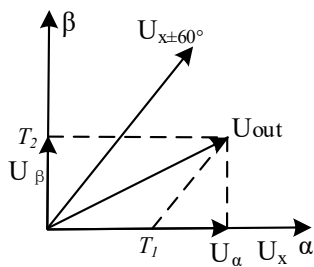


Fig. 3. Voltage vector decomposition diagram.

The calculation and judgment of the sector number in which the composite reference voltage vector is located is the first step of the SVPWM, and only the sector number can be selected to select the appropriate adjacent sector and the base vector. Firstly we assume:

$$\begin{cases} v_a = u_\beta \\ v_b = (\sqrt{3}u_\alpha - u_\beta) / 2 \\ v_c = (-\sqrt{3}u_\alpha - u_\beta) / 2 \end{cases} \quad (19)$$

$$N = \sin(v_a) + 2 \sin(v_b) + 4 \sin(v_c) \quad (20)$$

Then, the sector number can be determined based on the calculated N value:

Table 1. N and the corresponding number of sectors.

N	1	2	3	4	5	6
Sector number	II	VI	I	IV	III	V

To determine the component action time T_1 and T_2 of the voltage vector, we can assume that the required composite voltage vector is u , and then obtain the following relationship:

$$\begin{cases} T = T_0 + T_1 + T_2 \\ u = \frac{T_1}{T} u_1 + \frac{T_2}{T} u_2 \end{cases} \quad (21)$$

where T is the period and T_0 is the zero vector action time. After the composite voltage vector u is decomposed, equation (22) can be obtained:

$$\begin{cases} u_\alpha = \frac{T_1}{T} |u_1| + \frac{T_2}{T} |u_2| \cos \frac{\pi}{3} \\ u_\beta = \frac{T_2}{T} |u_2| \cos \frac{\pi}{3} \end{cases} \quad (22)$$

Equation (23) can be derived from the above formula:

$$\begin{cases} T_1 = \frac{T}{2U_{dc}} (3u_\alpha - \sqrt{3}u_\beta) \\ T_2 = \frac{T}{U_{dc}} \sqrt{3}u_\beta \end{cases} \quad (23)$$

For further calculation, and reasonable allocation of vector action time, the general variables X , Y , and Z are introduced.

$$\begin{cases} X = \frac{\sqrt{3}T_s}{U_{dc}} u_\beta \\ Y = \frac{T_s}{2U_{dc}} (3u_\alpha + \sqrt{3}u_\beta) \\ Z = \frac{T_s}{2U_{dc}} (-3u_\alpha + \sqrt{3}u_\beta) \end{cases} \quad (24)$$

The correspondence between N and the time T_1 and T_2 are shown in the following table:

Table 2. N and corresponding effect time.

N	I	II	III	IV	V	VI
T1	Z	Y	-Z	-X	X	-Y
T2	Y	-X	X	Z	-Y	-Z

After the SVPWM has obtained the voltage action time, it is necessary to determine at which point the action begins. According to the seven-segment symmetric modulation principle, the vector switching point can be obtained:

$$\begin{cases} T_a = (T_s - T_1 - T_2) / 4 \\ T_b = T_a + T_1 / 2 \\ T_c = T_b + T_2 / 2 \end{cases} \quad (25)$$

Table 3. Calculation of vector points TCMPx.

N	I	II	III	IV	V	VI
TCMP1	Tb	Ta	Ta	Tc	Tc	Tb
TCMP2	Ta	Tc	Tb	Tb	Ta	Tc
TCMP3	Tc	Tb	Tc	Ta	Tb	Ta

According to the above equations, a PMLSM mathematical model can be established in the $d-q$ coordinate system. Due to the principle of a linear motor and the control requirements, the $i_d = 0$ principle of the mover flux linkage is proposed in this paper. The electromagnetic torque is only proportional to the stator current in this method. So that the stator windings and the d shaft are completely independent and the linear motor model is further simplified. Based on the SVPWM, a three-loop vector control system of position loop, velocity loop and current loop is established. The control model is simplified by Park transformation and Clark transformation. The on-off mode of IGBT inverters is

decided by PWM signal that achieves vector control of PMLSM. The block diagram of the control system is shown in Fig.4.

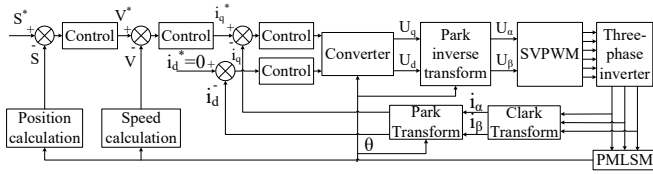


Fig. 4. Block diagram of the control system for a PMLSM.

The steps of the detail control scheme are as follows. When controlling the position of the motor mover, firstly we set a target position value S^* and compare the actual position S of the moral mover measured by the grating ruler to obtain the position deviation value. And then we input the position deviation value into the position controller, the output value can be calculated. The target speed value V^* is compared with the actual speed value V of the mover, and the obtained speed deviation value is sent to the speed controller. At last, the target control current I^* is calculated. Here, the target control current is composed of the d -axis current i_d and the q -axis current i_q . This design uses the control of $i_d = 0$, that is, the d -axis current i_d is equal to 0, and only the q -axis current i_q is to be controlled because the controlled current is only the i_q current component in the d - q coordinate system.

After the value of the target control current is obtained, it needs to be compared with the actual current. Since the actual current in the system is obtained by measuring the currents i_a, i_b, i_c in the three-phase stator of the motor through the Hall sensor, it is necessary to first calculate the currents i_d and i_q of the measured three-phase current in the d - q axis coordinate system by using the coordinate transformation method with Clark transform and Park transform described in (26).

$$\begin{bmatrix} i_d \\ i_q \end{bmatrix} = T_{3s/2r} \begin{bmatrix} i_a \\ i_b \\ i_c \end{bmatrix} \quad (26)$$

where $T_{3s/2r}$ is the transformation matrix of the synchronous motor three-phase stationary coordinate system converted into a two-phase rotating coordinate system. After i_d and i_q are obtained, they are respectively compared with the set values, and the deviation is sent to the current regulator to obtain the desired voltages u_d and u_q in the d - q axis coordinate system. Aand then u_d and u_q are converted to the two-phase stationary coordinate system. The transformation formula is as shown in (27).

$$\begin{bmatrix} u_\alpha \\ u_\beta \end{bmatrix} = T_{2s/2r}^{-1} \begin{bmatrix} u_d \\ u_q \end{bmatrix} = \begin{bmatrix} \cos \omega t & -\sin \omega t \\ \sin \omega t & \cos \omega t \end{bmatrix} \begin{bmatrix} u_d \\ u_q \end{bmatrix} \quad (27)$$

After u_α and u_β are obtained, they are modulated by the SVPWM algorithm and input to the inverter. The inverter acts on the motor to complete a current control. The current loop is in the innermost layer of the three control loops in the system, and its dynamic response speed is the fastest. Generally, the current loop control period is equal to the

carrier cycle of SVPWM. The speed loop is the middle layer control loop of the system. The speed loop needs to compare with the set value according to the detected speed value, and the difference value is applied by the speed regulator to obtain the desired current i_{qref} in the q -axis. The position loop is the outermost control loop of the system, and its response speed is slower than the speed loop, otherwise, it may cause the system to oscillate. The position loop is compared with the set value based on the detected actual position, and the difference is applied by the position adjuster to obtain the desired speed value.

For the linear motor servo control, especially for the control accuracy, the design needs to consider the adaptability to complex control objects and good dynamic response capability. For those purposes, researchers usually use new materials and processes to manufacture motors and explore ways to use more effective intelligent control strategies. In this work, a linear motor is the main research object, and some researches have been carried out from the linear motor control strategy to the bio-intelligence field. The controller in this system is the improved single neuron PID controller to be introduced in the following section of this paper.

3. IMPROVED SINGLE NEURON PID CONTROL

3.1 Single neuron PID controller

The traditional PID control is not suitable for dealing with the nonlinear and time-varying system due to its fixed control parameters. Those key parameters such as proportion, integral and differential coefficient need pre-set based on experimental data and continuous debug. In practical applications, the control algorithm also enables the control algorithm to adjust the control parameters in real-time and effectively respond to complex control objects, such as linear motors (Kwon et al., 1999; Zhu and Cho, 2007; Vaez-Zadeh and Isfahani, 2007; Ogawa et al., 2017). Taking advantage of the self-learning ability and self-adapting ability of neuron algorithm, and combining the algorithm with PID controller (Guo and Yu, 2005; Tabatabaei, 2016; Ilten and Demirtas, 2016), the improved single neuron PID controller is designed. The combination makes it possible to adjust PID parameters online according to the change of the control object. So the control system may obtain good adaptability and strong robustness. The block diagram of the single neuron PID control system is shown in Fig. 5.

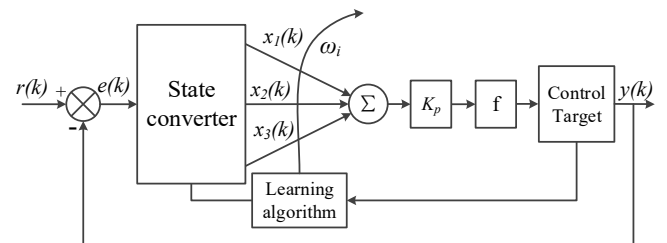


Fig. 5. Single neuron PID controller.

In Fig.5, $r(k)$ is the given value of the system. $e(k) = r(k) - y(k)$ is the definition error with the difference between the actual output and the expected value, which is also the input value of the state transfer. The single neuron PID controller has the

following main parameters: x_i and ω_i ($i=1, 2, 3$). They are controller input and corresponding connection weight coefficient respectively. K_p is the neuron proportional coefficient. f is the neuron activation function. There are three input signals in the control system $x_1(k)$, $x_2(k)$, and $x_3(k)$. And we can get the following equations:

$$\begin{cases} x_1(k) = r(k) - y(k) = e(k) \\ x_2(k) = e(k) - e(k-1) \\ x_3(k) = e(k) - 2e(k-1) + e(k-2) \end{cases} \quad (28)$$

Combining the unsupervised Hebb learning rules with the supervised delta learning rule, then we can get supervised Hebb learning rules:

$$\Delta w_{ij}(k) = \eta(d_j(k) - o_j(k))o_j(k)o_i(k) \quad (29)$$

The corresponding learning algorithm is (30) and (31):

$$\begin{aligned} \Delta u(k) &= K_p \sum_{i=1}^3 \omega_i(k)x_i(k) \\ &= K_p \{ \omega_1(k)e(k) + \omega_2(k)\Delta e(k) + \omega_3\Delta^2 e(k) \} \end{aligned} \quad (30)$$

$$\begin{cases} \omega_1(k) = \omega_1(k-1) + \eta_I z(k)u(k)x_1(k) \\ \omega_2(k) = \omega_2(k-1) + \eta_P z(k)u(k)x_2(k) \\ \omega_3(k) = \omega_3(k-1) + \eta_D z(k)u(k)x_3(k) \end{cases} \quad (31)$$

where K_p is the proportion coefficient of neurons ($K_p > 0$). And η_I , η_P , and η_D are integral, proportional and differential learning rates respectively. The neuron control algorithm has a good ability to adjust, which means that the algorithm structure adapts to the interference change of the control system through continuous learning (Pan and Luo, 2005).

3.2 Optimization of neuron weighting coefficients

In order to further optimize the learning algorithm, an inertial term $\xi_i[\omega_i(k-1) - \omega_i(k-1)^2]$ is introduced in this paper. ξ_i is the inertia coefficient and $0 < \xi_i < 1$. The inertial terms contribute to the stability of a single neuron algorithm in the process of iterative convergence and accelerate the convergence speed. The adjustment equations of neuron weighted coefficient are:

$$\begin{cases} \omega_1(k) = \omega_1(k-1) + \eta_I z(k)u(k)x_1(k) \\ \quad + \xi_1[\omega_1(k-1) - \omega_1(k-1)^2] \\ \omega_2(k) = \omega_2(k-1) + \eta_P z(k)u(k)x_2(k) \\ \quad + \xi_2[\omega_2(k-1) - \omega_2(k-1)^2] \\ \omega_3(k) = \omega_3(k-1) + \eta_D z(k)u(k)x_3(k) \\ \quad + \xi_3[\omega_3(k-1) - \omega_3(k-1)^2] \end{cases} \quad (32)$$

In addition, many practical applications show that the adaptive learning of the single neuron PID parameters is related to $e(k)$ and $\Delta e(k)$. Therefore the $x_i(k)$ ($i=1,2,3$) are segmentation processed here. When $|e(k)| \leq A$, the value $x_i(k)$ are as follows:

$$\begin{cases} x_1(k) = e(k) \\ x_2(k) = e(k) - e(k-1) \\ x_3(k) = \Delta^2 e(k) = e(k) - 2e(k-1) + e(k-2) \end{cases} \quad (33)$$

Otherwise, when $|e(k)| > A$, the value $x_i(k)$ is shown in (34).

$$x_i(k) = e(k) + \Delta e(k) \quad (34)$$

where the value A is determined empirically.

It can be concluded from the single neuron learning algorithm above, that the neuron proportional coefficient, learning rate and the initial value of the weighted coefficient are several key parameters in the design of a single neuron PID controller. The weighting coefficient is constantly adjusted, so the initial value can usually be any value. The learning rate has a large range after normalization. The value of the neuron proportional coefficient K_p will directly affect the dynamic response and stability of the control system. If K_p is large, the dynamic responses of the system perform well but the overshoot will be larger and the adjustment time will be longer. On the other hand, the system will respond slowly and the overshoot will be smaller, which may cause a serious lag. In order to improve the response speed of a single neuron PID controller, this paper combines the biological cellular immune regulatory mechanism with the single neuron learning algorithm to adjust K_p dynamically.

3.3 Proportional coefficient optimization based on the immune regulation mechanism

A. Cellular immune regulatory mechanism

Cellular immunity is an important part of the immune system of an organism, which cooperates with humoral immunity to achieve specific immunity. Cellular immunity is mainly caused by a series of stress responses of thymus-dependent lymphocyte that is T cell population under the condition of antigen invasion and synergetic with B cells. The cell population mainly contains three types of cell subpopulation, auxiliary T cells that are T_H cells have a role in promoting the promotion; cytotoxic T cells that are T_c cells have the role of eliminating target cells and inhibit T cells that is T_s cells with the function of inhibition. Three types of cell subgroups participate in the process of three stages of cellular immune and maintain the balance of the biological immune system through their interaction (Hou and Wang, 2009; Bouchebbat and Gherbi, 2017).

At different moments of cellular immune regulation, the roles of the three T cell subgroups are different. In the early stage, antigen concentration is larger and antibody concentration is small, and the T_H cells promote the immune process, which stimulates T lymphocyte to differentiate T_c and activate B cells. In the later, with the decrease of the antigen concentration and the increase of the antibody concentration, T_s cells inhibit the production of other kinds of lymphocytes to complete the immunomodulatory and avoid immunosuppression or immunosensitivity caused by

disorders of the immune system. The role of T cell population during immunomodulation is shown in Table 4.

Table 4. The function of T cells in immune adjustment

Immune regulation process	Antigen concentration	Antibody concentration	T cell effect
Antigen invasion	Heavy	Very Light	/
The early period of immunization	Heavy	Light	Promote
The later period of immunization	Light	Heavy	Inhibition
Rest Immune stability	Very Light	Light	/

According to the mechanism of immune regulation, we can get the cell concentration of k generation B cells by simplifying the T_H cell, T_C cell, T_S cell, and B cell interaction:

$$B(k) = T_H(k) + T_C(k) - T_S(k) \quad (35)$$

$$T_H(k) = k_1 \varepsilon(k) \quad (36)$$

$$T_C(k) = k_2 f[B(k-1)] \varepsilon(k) \quad (37)$$

$$T_S(k) = k_3 f[B(k)] \varepsilon(k) \quad (38)$$

where the k generation antigen concentration is defined as $\varepsilon(k)$. The output of the antigen-stimulated T_H cell is defined as $T_H(k)$. The stimulation of B cells by T_c cells is defined as $T_c(k)$. The stimulation of B cells by T_s cells is defined as $T_s(k)$. And k_1 , k_2 , and k_3 are the corresponding inhibitors $f(\cdot)$, a non-linear function, represents the effect of the immune of B cells in the k generation. Correspondingly, there is the following relationship between B cell concentration $B(k)$ and the antigen concentration $\varepsilon(k)$:

$$B(k) = k_1 \varepsilon(k) + k_2 \{f[B(k-1)]\} \varepsilon(k) - k_3 \{f[B(k)]\} \varepsilon(k) \quad (39)$$

$$= K_b \{1 + f[B(k-1)] - f[B(k)]\} \varepsilon(k)$$

where $K_b = k_1 + k_2 - k_3$.

Modulation of the immune system maximizes the protection of organisms by eliminating the presence of antibodies while avoiding excessive levels of antibodies that can cause adverse effects on the organism. The dynamic adjustment process of the control system is similar to the immune system regulation, which has the ability to quickly eliminate the deviation and ensure the stable operation of the system.

B. Design of the immune controller

Making the antigen concentration $\varepsilon(k)$ as the systematic bias and the overall impact of B cells as the system input, then we can get the feedback control output:

$$u(k) = K_c \{1 + \lambda f[u(k-1)] - \lambda f[(u(k))]\} \varepsilon(k) \quad (40)$$

where $\lambda = (-1, 0, 1)$ is an immune promotion, immune stability and immune suppression in three stages of the response

process respectively. $y_r(k)$ is the given output of the control system. $y(k)$ is the actual output of the control system, and $e(k) = y_r(k) - y(k)$. The immune controller structure is shown in Fig.6.

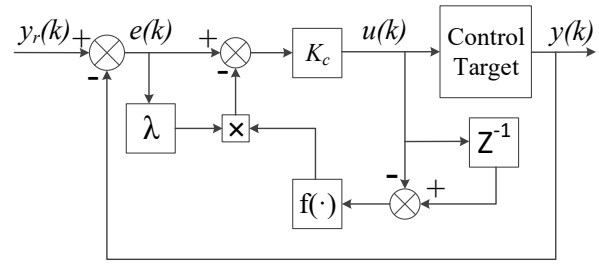


Fig. 6. Structure of the immune-based controller.

C. Design of the cell regulation function

According to the regulatory role of the T cell, we can select the regulating function, the function graph is as follows.

$$f(x) = \left| \frac{2}{1 + \exp(-2x)} - 1 \right| \quad (41)$$

During the immune boost phase $\lambda = -1$, the controller gain is:

$$K_c \{1 + \lambda f[u(k-1)] - \lambda f[u(k)]\} \rightarrow K_c \{1 - f[u(k-1)] + f[u(k)]\} \quad (42)$$

During the immunosuppressive phase $\lambda = 1$, the controller gain is:

$$K_c \{1 + \lambda f[u(k-1)] - \lambda f[u(k)]\} \rightarrow K_c \{1 + f[u(k-1)] - f[u(k)]\} \quad (43)$$

During the immune stability phase $\lambda = 0$, the controller gain is:

$$K_c \{1 - \lambda f[u(k-1)] - \lambda f[u(k)]\} \rightarrow K_c \quad (44)$$

D. Neuron proportional coefficient adjustment

In order to make the neuron proportional coefficient have better adaptability to the single neuron PID algorithm, it should be adjusted online according to the systematic error. During the control process in the early stage, the value of K_p in initial stage should be large to adjust the system rapidly. After the later stage, the value of K_p needs to be gradually adjusted and reduced to a stable value. With the immune regulator and the regulating function, the system adjustment process is segmented. Then the adjustment rules of K_p in the improved single-neuron PID control algorithm are as follows:

$$\begin{cases} K_p = K_c \{ [1 - f[u(k-1)] + f[e(k)]] \} \\ \quad \text{(when } e_0 < e(k) \leq e_1) \\ K_p = K_c \{ [1 + f[u(k-1)] - f[e(k)]] \} \\ \quad \text{(when } e_1 < e(k) \leq e_2) \\ K_p = K_c \\ \quad \text{(when } e_2 < e(k) \leq e_3) \end{cases} \quad (45)$$

$$K_c = \alpha + \beta e(k) \tag{46}$$

where $e_0, e_1, e_2,$ and e_3 are chosen by experts' experience. Also in order to make the controller have a stronger online self-adaptive ability, we lead into the variables α and β to adjust the initial proportion coefficient K_c and make its value suitable.

4. RESULTS AND DISCUSSIONS

The control structure of system hardware for a PMLSM is designed and shown in Fig. 7. The system includes the main circuit, control circuit, detection circuit, protection circuit, and a PMLSM, etc. The DSP processor is designed as the core chip to complete the three-loop control of the linear motor, as well as the generation of the SVPWM waveform and the realization of the intelligent controller based on the proposed algorithm (Li et al., 2005; Wang et al., 2015). The intelligent power module (IPM) is used in the inverter circuit for power conversion. Grating rules and Hall sensors are used for the position and current detection of the linear motor.

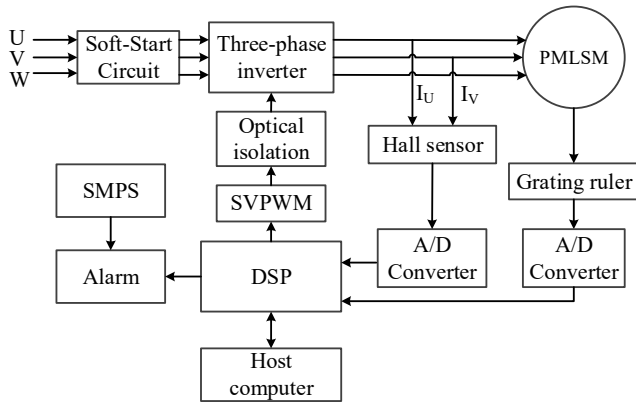


Fig. 7. Structure of control system hardware.

The variables of the linear motor are set as follows: the number of pole pair $P = 3$, permanent magnet flux linkage $\psi_f = 0.049$ Wb, the inductance of d shaft $L_d = 0.047$ H, inductance of q shaft $L_q = 0.067$ H, stator resistance $R = 3.05 \Omega$, pitch $\tau = 52.2$ mm, mover mass $M = 6.0$ kg and friction coefficient $B = 0.001(N \times s/m)^{-1}$. In the simulation, the expected displacement of the linear motor is set to be 5.0 m. The single neuron PID control and the improved single neuron PID control proposed in this paper are respectively used in the system to test the control performance. The results are shown in Fig.8. The dashed blue curve (SN-PID) is the response curve of the single neuron PID control, and the solid red curve (ISN-PID) is the response curve of the improved single neuron PID control. It can be seen from the figure that the response curve using the improved single neuron PID control reaches the desired value at 0.5 s, whereas the response curve using the single neuron PID control lags significantly.

The analysis of the motor thrust is also shown in Fig.9. compared with the single neuron PID control (dashed blue line, SN-PID), the thrust waveform of the improved single neuron PID control (solid red line, ISN-PID) has obvious jerkiness and smaller jitters amplitude in the control process,

which proving the control of the control method has the advantage from the other side.

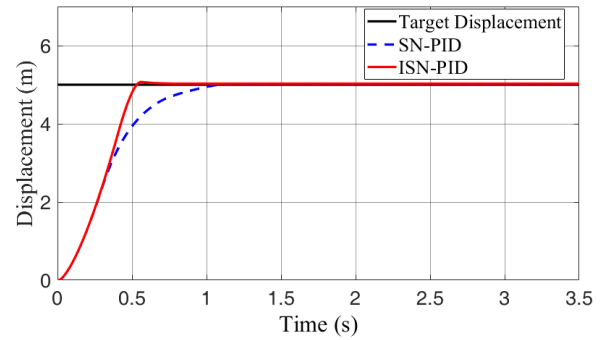


Fig. 8. Displacement response curve at the step response.

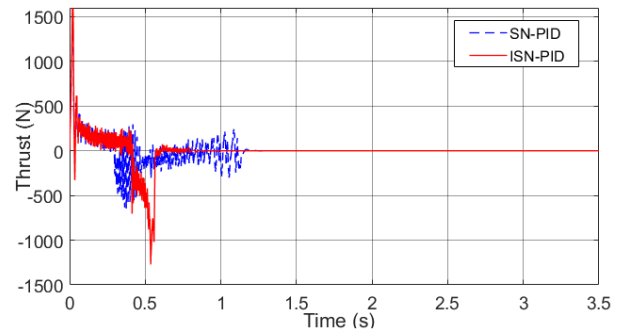


Fig. 9. Motor thrust waveform.

For a better comparison of the response performance of two controllers, another experiment was performed. The expected displacement of the linear motor is set to be 5.0 m, and a fast-displacement adjustment (8.0 m) is set from 1.0 s to 2.0 s, and then set back to 5.0 m. The experiment results are shown in Fig.10. It can be seen that the response curve of the improved single neuron PID control (solid red line, ISN-PID) can achieve the expected value quickly and return to the initial state with certain rapid adaptability. In contrast, the response curve using the single neuron PID control (dashed blue line, SN-PID) cannot fully reach the target of the predetermined displacement and it is hard to return to the original setting state.

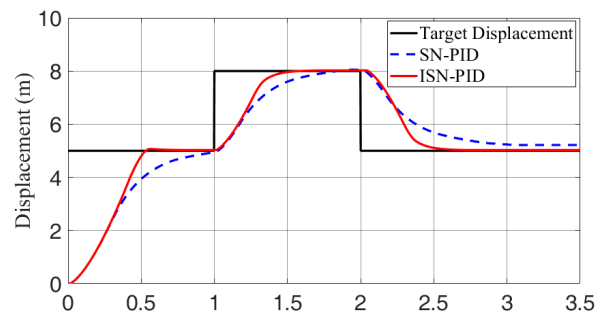


Fig. 10. Displacement response curve.

In order to verify the anti-jamming and stability control capabilities with the improved single neuron PID control, the unequal amplitude of the square wave signal and the interference signal are set to the linear motor speed control. The result is shown in Fig.11. The dashed blue curve (SN-PID) is the response curve of the single neuron PID control,

and the solid red curve (ISN-PID) is the response curve of the improved single neuron PID control. In the first 0.3 seconds, we set the motor to move forward, and the speed is positive. The motor speed is set to be negative in 0.4 seconds, and the motor moves backward. It can be seen from the waveform that the speed signal changes at 0.1 s, 0.2 s, 0.3 s and 0.4 s respectively. According to the result of the comparison, when the velocity varies in different amplitudes and direction, the single neuron PID control takes longer to track the given value and in some cases cannot reach the expected value all the time. In addition, Fig. 12 shows the result of the thrust of the motor in the above experiment. The motor thrust waveform with the improved single neuron PID control has a more accurate and faster response with a smaller fluctuation every time the motor operating status changes, which shows that the motor operation control adjustment is more stable and effective.

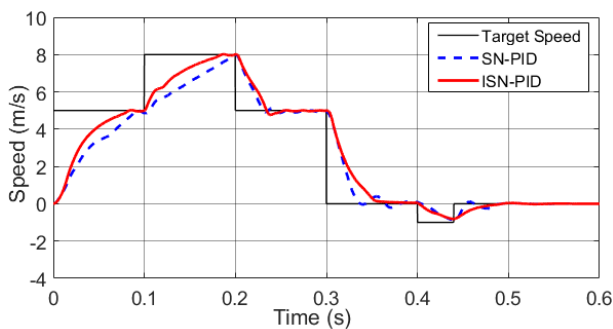


Fig. 11. Speed response curve.

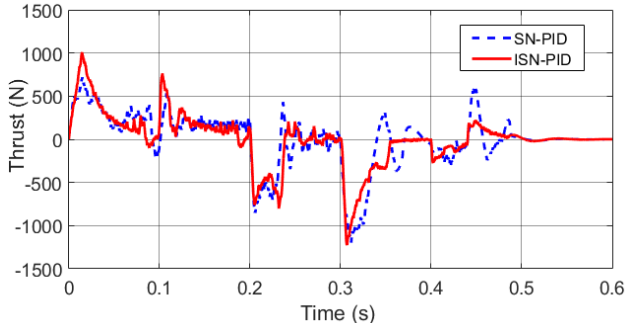


Fig. 12. Motor thrust waveform.

5. CONCLUSIONS

As a new widely-used motor, a PMLSM has many advantages of being applied to the field of precision machine tools, intelligent production, and modern transportation. However, there are some other characteristics such as nonlinearity, strong coupling, and multi-control variables, etc. In practical applications, the most common use is to control the speed and position accuracy of the motor. Usually, the control method is PID control technology, which is widely used in linear non-time-varying control objects. This method has the advantages of simple structure and easy adjustment of parameters. However, the traditional PID control is not suitable for dealing with the nonlinear and time-varying system due to its fixed control parameters. In the actual use process, it is necessary to rely on certain experiences and a large amount of experimental data to

obtain the set control parameters. With the application of nonlinear and complex control objects in practice, it has been difficult to meet the requirements of high precision and fast response of the control system. Therefore, many improved methods for PID control have been proposed to improve the control adaptability. The proposed PMLSM control is designed in this paper based on SVPWM, by optimizing the traditional principle model of a PMLSM and using the improved single neuron PID. The biggest feature of the proposed control algorithm is the ability to cope with complex and varied system's internal and external changes with good self-learning and self-adaptive capabilities.

According to the structure and working principle of a PMLSM, the mathematical model is set up by using the space vector control method and coordinate transformation, and the corresponding control system is built by SVPWM with $i_d = 0$ methods. Combining biological cellular immune regulation and single neuron PID control algorithm, an improved single neuron PID control algorithm is proposed to optimize the neuron weighting coefficient and enhance the stability of the iterative convergence process. The immunomodulatory mechanism that can eliminate antigen to steady the immune system have been used. And the immunomodulatory algorithm is introduced to adjust the neuron coefficient online to improve the learning speed of the neuron algorithm and adjust the proportion coefficient value online. It alleviates the low learning efficiency and long response time of the ordinary single neuron PID controller. In the case of the motor servo control, some steps are needed for practical application. Firstly, the model of the control system should be built by SVPWM with $i_d = 0$ methods. Second, according to the actual application needs, one can build the hardware system structure of the entire motor control. Lastly, the control algorithm proposed in this paper is used in the software design of the control system.

The method proposed in this paper can not only improve the learning speed of the neuron algorithm but also adjust the value of the proportional coefficient online. The experimental results show that the improved single-neuron PID control is more robust and traceable than the single-neuron PID control when applied in the vector control system of a PMLSM. The proposed control algorithm is fast, stable and accurate from the principle and result. It will be helpful to provide a good reference for further research. In the next study, we will further analyze the theory and continuously improve the structure of the control system.

ACKNOWLEDGEMENTS

This work is supported by the Fundamental Research Funds for the Central Universities (Grant No. JZ2019HGTB0082), and the National Natural Science Foundation of China (Grant Nos. 51505120 and 11105028). The support provided by the China Scholarship Council (CSC) is also acknowledged.

REFERENCES

An HJ, Cho GW, Jang KB, & Kim GT. The Improved Design of Double Sided Core less PMLSM with Consideration of Rising Winding Temperature. *J Electr Eng Technol*

- 2013;8:144-149.
- Bahmanpour M, Koofigar HR, Delshad M, & Tosifian MH. Nonlinear Control and Implementation of a Hybrid Power System. *Control Eng Appl Inform* 2019;21:70-78.
- Bashir AO, Rui XT, Abbas LK, & Zhang JS. Ride Comfort Enhancement of Semi-active Vehicle Suspension Based on SMC with PID Sliding Surface Parameters Tuning using PSO. *Control Eng Appl Inform* 2019;21:51-62.
- Biswas S, Dong Q, Rafalko V, & Rimmele A. Dynamic Model-Based Vector Control of Linear Induction Motors. *Nav Eng J* 2013;125:127-134.
- Boldea I, & Nasar SA. Linear electric actuators and generators. *Ieee T Energy Conver* 1999;14:712-717.
- Bouchebbat R, & Gherbi S. Design and application of fuzzy immune PID adaptive control based on particle swarm optimization in thermal power plants. In: Drid S, Mehdi D & Aitouche A editors. *2017 6th International Conference on Systems and Control. New York: Ieee;* 2017. p. 33-38.
- Butt CB, Hoque MA, & Rahman AA. Simplified fuzzy-logic-based MTPA speed control of IPMSM drive. *Ieee T Ind Appl* 2004;40:1529-1535.
- Butt CB, & Rahman MA. Intelligent Speed Control of Interior Permanent Magnet Motor Drives Using a Single Untrained Artificial Neuron. *Ieee T Ind Appl* 2013;49:1836-1843.
- Cash S, & Olatunbosun O. Fuzzy logic field-oriented control of an induction motor and a permanent magnet synchronous motor for hybrid/electric vehicle traction applications. *Int J Electr Hybrid Veh* 2017;9:269-284.
- Dang DQ, Vu NTT, Choi HH, & Jung JW. Neuro-Fuzzy Control of Interior Permanent Magnet Synchronous Motors: Stability Analysis and Implementation. *J Electr Eng Technol* 2013;8:1439-1450.
- Durand S, Boisseau B, Marchand N, & Guerrero-Castellanos JF. Event-Based PID Control: Application to a Mini Quadrotor Helicopter. *Control Eng Appl Inform* 2018;20:36-47.
- Giernacki W, Horla D, Sadalla T, & Fraire TE. Optimal Tuning of Fractional Order Controllers for Rotational Speed Control of UAV's Propulsion Unit Based on an Iterative Batch Method. *Control Eng Appl Inform* 2018;20:22-31.
- Giernacki W, & Sadalla T. Comparison of Tracking Performance and Robustness of Simplified Models of Multirotor UAV's Propulsion Unit with CDM and PID Controllers (with anti-windup compensation). *Control Eng Appl Inform* 2017;19:31-40.
- Guo BJ, & Yu JS. A single-neuron PID adaptive multicontroller scheme based on RBFNN. *T I Meas Control* 2005;27:243-259.
- Hellinger R, & Mnich P. Linear Motor-Powered Transportation: History, Present Status, and Future Outlook. *P Ieee* 2009;97:1892-1900.
- Hou YH, & Wang YH. Based on Neuron adaptive Controller for Linear Motor Slip Frequency Vector Control System. In: Tang YC, Lawry J & Huynh VN editors. *2009 International Conference on Intelligent Human-Machine Systems and Cybernetics, Vol 2, Proceedings. Los Alamitos: Ieee Computer Soc;* 2009. p. 94-98.
- Ilten E, & Demirtas M. Off-Line Tuning of Fractional Order PI lambda Controller by Using Response Surface Method for Induction Motor Speed Control. *Control Eng Appl Inform* 2016;18:20-27.
- Jia YF, Zhou ZQ, Xue KX, Zhao L, & Cai KY. Using Neural Networks to Forecast Available System Resources: An Approach and Empirical Investigation. *Int J Softw Eng Know* 2015;25:781-802.
- Jones K, Williams D, & Goodier A. Auto-tuning PID control of dissolved oxygen in a *Saccharomyces cerevisiae* fermentation. *Meas Control-uk* 1996;29:266-269.
- Kim YH, Kim WK, & Kim S. Maximum Power Control of IPMSM Considering Nonlinear Cross-Magnetization Effects. *J Electr Eng Technol* 2012;7:940-947.
- Kwon BI, Woo KI, & Kim S. Finite element analysis of direct thrust-controlled linear induction motor. *Ieee T Magn* 1999;35:1306-1309.
- Li HZ, Gong Z, Lin W, Jiang TY, & Chen XQ. DSP-based motion control of a non-commutated DC linear motor module. *Int J Softw Eng Know* 2005;15:313-318.
- Marzi H. High-speed RT monitoring system using neural networks. *Int J Softw Eng Know* 2005;15:439-445.
- Ogawa H, Tanaka R, Murakami T, & Ishida Y. Two-Stage Control System of a DC Motor using Dual-Sampling Observer. *Control Eng Appl Inform* 2017;19:59-66.
- Oto Y, Noguchi T, Sasaya T, Yamada T, & Kazaoka R. Space Vector Modulation of Dual-Inverter System Focusing on Improvement of Multilevel Voltage Waveforms. *Ieee T Ind Electron* 2019;66:9139-9148.
- Pan ZY, & Luo FL. Steady state reference current determination technique for brushless DC motor drive system. *Ieee P-elect Pow Appl* 2005;152:1585-1594.
- Pelc M. Context-aware Fuzzy Control Systems. *Int J Softw Eng Know* 2014;24:825-856.
- Ramasamy P, Krishnasamy V, Sathik MAJ, Ali ZM, & Aleem S. Three-Dimensional Space Vector Modulation Strategy for Capacitor Balancing in Split Inductor Neutral-Point Clamped Multilevel Inverters. *J Circuit Syst Comp* 2018;27:20.
- Saleem O, Hassan H, Khan A, & Javaid U. Adaptive Fuzzy-PD Tracking Controller for Optimal Visual-Servoing of Wheeled Mobile Robots. *Control Eng Appl Inform* 2017;19:58-68.
- Saleem O, Shami UT, Mahmood-ul-Hasan K, Abbas F, & Mahmood S. Robust-Optimal Output-Voltage Control of Buck Converter using Fuzzy Adaptive Weighted Combination of Linear Feedback Controllers. *Control Eng Appl Inform* 2019;21:43-53.
- Setayeshi S, Rad VB, Noruzi A, & Yousefi N. Optimal Design of Wide Area Based on Fuzzy Controller and Intelligent Method. *Int J Softw Eng Know* 2017;27:449-473.
- Shankar M, & Devi RPK. Choice of Frequency Ratio and Its Optimization for PWM Inverter Harmonic Distortion Control. *Control Eng Appl Inform* 2019;21:31-41.
- Tabatabaei M. PID Controller Design Based on Laguerre Orthonormal Functions. *Control Eng Appl Inform* 2016;18:65-76.
- Tang CS, & Duan ZY. Direct thrust-controlled PMSLM servo system based on back-stepping control. *IEEJ Trans*

- Electr Electron Eng* 2018;13:785-790.
- Torres FJ, Guerrero GV, Garcia CD, Valencia G, Claudio A, & Mina JD. Task-Space Synchronization of Robot Manipulators Driven by Three-Phase Induction Motors. *Control Eng Appl Inform* 2019;21:63-70.
- Ullah S, Khan Q, Mehmood A, & Akmeliawati R. Integral backstepping integral sliding mode control of underactuated nonlinear electromechanical systems. *Control Eng Appl Inform* 2019;21:42-50.
- Vaez-Zadeh S, & Isfahani AH. Enhanced modeling of linear permanent-magnet synchronous motors. *Ieee T Magn* 2007;43:33-39.
- Wang JB, & Howe D. Design optimization of radially magnetized, iron-cored, tubular permanent-magnet machines and drive systems. *Ieee T Magn* 2004;40:3262-3277.
- Wang W, Xu LH, & Hu HG. Neuron adaptive PID control for greenhouse environment. *J Ind Prod Eng* 2015;32:291-297.
- Wei W, Wang YH, & Wang SR. A Speed Control System of Permanent Magnet Linear Synchronous Motor Using Neuron Adaptive Controller. *Los Alamitos: Ieee Computer Soc*; 2009.
- Yan LG. The Linear Motor Powered Transportation Development and Application in China. *P Ieee* 2009;97:1872-1880.
- Zhu YW, & Cho YH. Thrust ripples suppression of permanent magnet linear synchronous motor. *Ieee T Magn* 2007;43:2537-2539.